Correlation of High Energy Proton and Atmospheric Neutron Destructive and Non-Destructive Single-Event Effect Tests of a 1200V SiC MOSFET

H. Rizk, C. Ngom, V. Pouget, A. Michez, F. Lachaud, G. Le Morvan, F. Miller, M. Zerarka, O. Perrotin, F. Coccetti

***Abstract*—.We present the correlation of high energy proton and atmospheric neutron single-event test results on a recent 1200V SiC MOSFET, obtained with destructive and non-destructive methods. The correlation of the results is discussed, showing a good agreement between both methods. TCAD modelling is used to investigate the failure mechanisms.**

***Index Terms*—single-event effects, silicon carbide, power device, cross section.**

I. INTRODUCTION

Silicon carbide (SiC) MOSFETs have made considerable progress in process maturity and performances in the last decade and the recent generations of these devices are now considered as reliable alternatives to Si technologies for high-voltage power applications, a move motivated by the interesting electric and thermal properties of the SiC material that allow to design more efficient and more integrated power systems.

Regarding radiation effects, it has been demonstrated that SiC MOSFETs can be sensitive to destructive single-event effects and latent damages induced either by heavy ions in space applications or by secondary particles generated by neutrons from the atmospheric environment [1-5]. The details of the failure mechanism can vary depending on the technology details, the drain voltage and the particle properties, including leakage currents, single-event burn-out (SEB) and single-event gate rupture (SEGR) effects.

When testing for such effects in power devices for terrestrial applications, the standard approach is to apply a statistical destructive test method [6-7] using either an atmospheric-like neutron spectrum or high energy protons, in order to obtain a measurement of the destructive events cross section. For Si devices, an alternative non-destructive test method [8] based on single-event transients acquisitions has been shown to provide good results while reducing the test costs.

In this work, we perform measurements of the destructive single-event cross-section of a commercial 1200V SiC power MOSFET reference under high energy protons and atmospheric-like neutrons using a classical statistical destructive test method and non-destructive test method. The results of the different experiments are correlated, taking into account the neutron beam attenuation in a multiple test-boards setup.

This work was funded by the SiCRET project.

H Rizk was with IRT Saint Exupery, Toulouse, France and Institut d'Electronique et des Systemes (IES), University of Montpellier, CNRS (UMR5214), Montpellier France, and is now with Nuclétudes, Les Ulis, France

C. Ngom is with IRT Saint Exupery, Toulouse, France and Institut d'Electronique et des Systemes (IES), University of Montpellier, CNRS (UMR5214), Montpellier France.

V. Pouget and A. Michez are Institut d'Electronique et des Systemes (IES), University of Montpellier, CNRS (UMR5214), Montpellier France .

F. Lachaud, G. Le Morvan, F. Miller are with Nucletudes, Les Ulis, France.

M. Zerarka, O. Perrotin, F. Coccetti are with IRT Saint Exupery, Toulouse, France.

II. EXPERIMENTAL SETUP & METHOD

A. Device under test

The DUT is a commercial 1200V SiC power MOSFET of recent generation, with a classical vertical structure, interdigitated lines of source and gate contacts on the front-side, and drain contact on the substrate backside, with a TO-247 like plastic package.

B. Statistical destructive test method

In contrast with the case of non-destructive events where the cross-section is classically measured by counting the number of successive events in a single device as a function of the particle fluence, it is required to take into account that, with destructive events, once a component is destructed, it does not contribute anymore to the measurement process, and the random nature of a single-event does not allow any reliable extrapolation. This is where the statistical approach is required, which consists in testing a certain number of devices under the same beam and voltage conditions, while monitoring electrical observables to detect destructive events and logging the times-to-failure, i.e. the instants at which the events occur [6]. The higher the number of tested devices, the more reliable the measurement of the cross-section is [7]. Indeed, the variance on the mean time-to-failure is inversely proportional to the number of failures.

C. Non-destructive test method

Although the statistical test approach allows to get an accurate assessment of the destructive events cross section, it needs a large number of components to be tested and may require long beam time in the aimed facility (neutron, proton or heavy ion beams). These constraints increase the test costs. An alternative approach, which main advantage is to be non-destructive, was proposed and validated on Silicon power components in [8] . It relies on the study of what the authors call precursory single-event transients (SET), which are amplified SET that appear at the upper limit of the device safe operating area (SOA), as represented in Fig. 1. For these biasing conditions, parasitic structures and impact ionization phenomenon can be triggered but the conditions are still not met for the device to enter an electrical and then thermal runaway. It was demonstrated in [8] that these precursory SET would have been destructive (SEB) for higher biasing conditions.

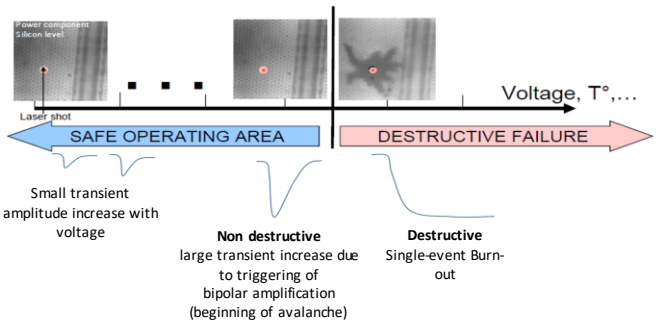

Fig. 1. Principle of the non-destructive test approach

The methodology then relies on applying a relatively low drain biasing on the component under beam and then, increasing it progressively according to a predefined voltage step. At the beginning, the observed transient signals have a small amplitude then this latter increases while increasing the applied drain voltage. At the limit of the SOA, the transients are not yet destructive; however, they last for a longer time and have a larger amplitude. By crossing the SOA, a destructive SEB could destroy the component at any time depending on the particle nature and energy, the device operating conditions (temperature, Vds, Vgs) and the strike point position.

The post experiment data processing allows to obtain, at first place, the SET occurrence as function of the SET rank for each tested drain voltage values. Then, these data are used to draw the evolution of the cross section as a function of the SET rank for each drain bias. At the end, all these curves are overlaid and the change in the slope indicates the cross section of the precursory SET, that is the expected saturated SEB cross section.

In the process of validating the electrical test set-up for this work, especially the amplifier section of the circuit to observe the SETs of interest, the proof of concept of the non-destructive test approach was first re-established on a 500V Silicon power MOSFET using backside single-photon absorption laser testing at Nucletudes facility. The results of this preliminary test are presented in Fig. 2 in the form of SET amplitude mappings for different drain voltages.

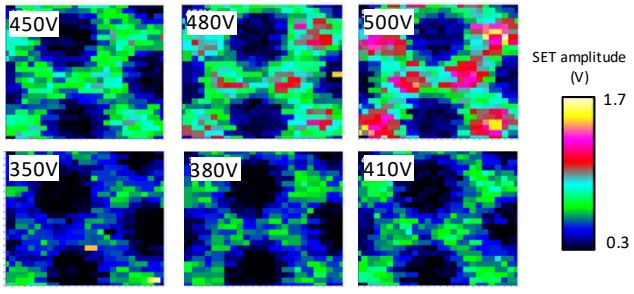

Fig. 2. Laser mapping of the precursory SET in a 500V Si power MOSFET

As it can be seen, only some locations exhibit a significant SET amplitude increase as a function of the biasing voltage. These are the locations triggering the precursory events which will lead to SEB for biasing voltages above the SOA. The mappings structure reveals the typical HEXFET geometry of this device [8]. The most sensitive locations are close to the channel whereas the less sensitive ones are in the source, where the injected charge is collected with no chance to trigger the parasitic transistor.

One of the challenges here is that for a similar rated voltage the depletion layer in SiC devices is thinner than for a Si counterpart. The impact is that the sensitive volume of SiC power devices is expected to be thinner compared to Si power devices for a similar rated voltage. As the sensitive volume is thinner, SETs are expected to have a smaller amplitude as well.

D. Electrical test setup

Fig.3 presents the experimental setup for the statistical destructive experiments. In order to test many DUTs in parallel under a particle while keeping the electrical setup simple, the gates and drains of all the DUTs are supplied in parallel by a single SMU for the gates and a high-voltage power supply for the drains. Series resistors limit the established current when a destructive event occurs, while capacitances act like transient local charge reservoirs that allow the failure mechanisms to be triggered despite the presence of the current-limiting resistors.

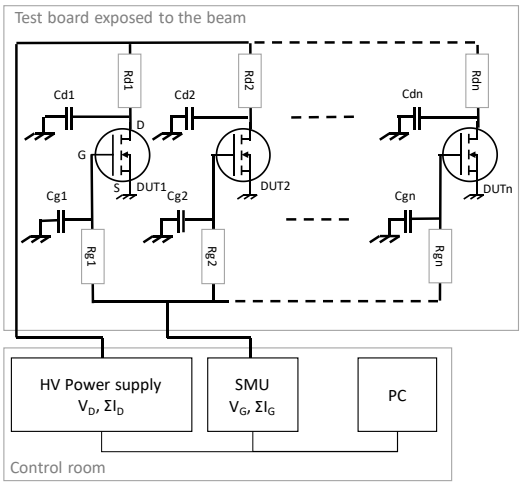

Fig. 3. Experimental setup for statistical destructive test

During the beam tests, the total currents are monitored and a destructive event resulting in a short between drain and source appears as a step on the total drain current measured by the HV power supply and/or on the total gate leakage current measured by the SMU.

For the non-destructive test method, the setup is similar to the one presented in [8], except that the choice was made to use

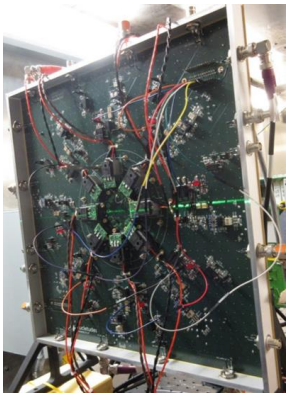

Fig. 4. Test board for non-destructive test approach (8 DUTs in the center)

an amplification stage since, as mentioned above, the SET amplitudes in the 1200V SiC power MOSFET were expected to be smaller than for the Si device studied in [8]. The test board allowing to test up to eight devices at once using the non-destructive method is represented in Fig. 4

E. Pre-irradiation characterization

The threshold voltage (Vth) and on-resistance (Rds_On) of all devices were characterized before irradiation using a well-defined preconditionning protocol to favor reproducible measurement. Fig. 5 presents the initial variability on these two parameters, which was found to be within the manufacturer specifications margins. Although no outlier was detected, it is interesting to notice a certain level of part-to-part variability that is not uncommon for this type of technology.

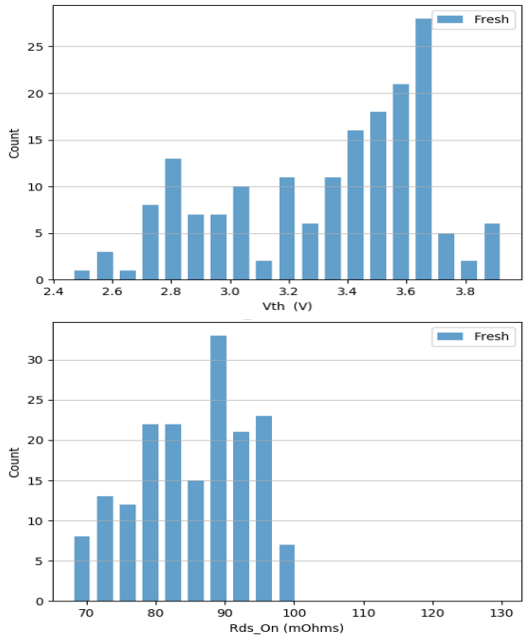

Fig. 5. Pre-irradiation characterization results.

F. Beam experiments setup and parameters

The high-energy proton test campaign was performed at Orsay Protontherapy Center (CPO) at an energy of 194MeV, and a maximum flux of 2.10^8 p.cm^{-2}.s^{-1}. Up to 8 devices per run were exposed in parallel within the beam diameter of 10cm (Fig. 6). Using the statistical destructive test setup, a first investigation run was performed while increasing Vds from 300 to 1200V per steps of 50V when the fluence reached 2.10^9 p.cm^{-2} for each Vds to get a rough estimate of the SOA. The upper limit of the SOA was determined to be close to 800V. Then, several statistical runs were performed at constant Vds of 800V and 850V up to a fluence of 10^{11} p.cm^{-2} for each run. Finally, runs were also performed unsing the non-destructive test method.

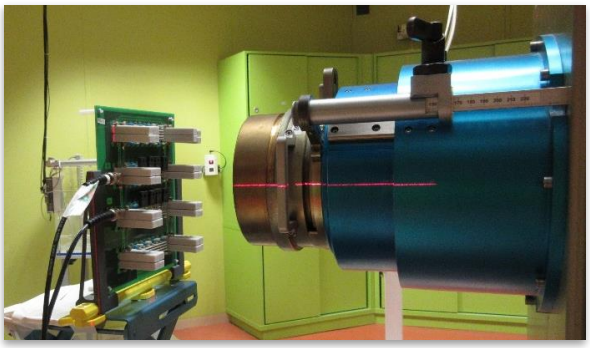

Fig. 6. Test board under high energy proton beam at CPO facility.

The neutron test campaigns were performed at ISIS ChipIR beamline, which provides an atmospheric-like energy spectrum up to 800MeV. In a first campaign, for the statistical destructive test method, 32 devices were exposed in parallel at Vds=850V up to a fluence of 8.10^{10} n.cm^{-2}. Non-destructive tests were performed on one device for biasing voltages between 825V and 950V. In this first campaign, multiple boards were stacked one behind another in the beam path as presented in Fig. 7.

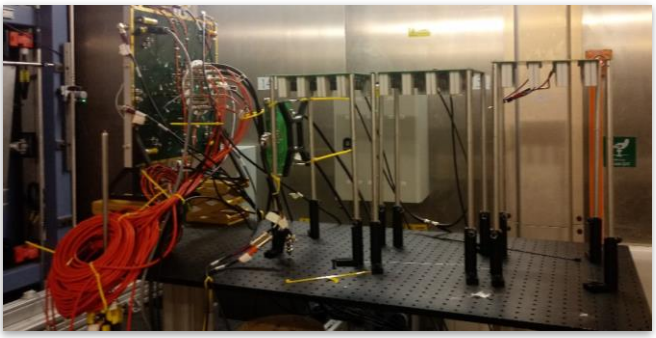

Fig. 7. Test boards setup for the first campaign under neutron beam at ISIS ChipIR facility. The beam output is on the left side of the picture. DUTs in this work are positioned on the first and third board from the left.

During a second neutron test campaign, the destructive test method was used at Vds=1050V with the test boards facing the beam, without being stacked (Fig.8).

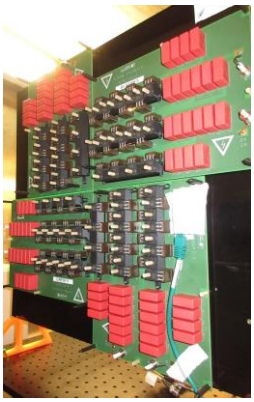

Fig. 8. Test boards setup for the second campaign at ISIS ChipIR facility, with all DUTs positioned in the same plane for the statistical test approach.

III. EXPERIMENTAL RESULTS

A. High energy proton destructive test results

Fig. 9 presents the Weibull plots of the results for the proton test of 24 devices at 850V and 16 devices at 800V. A fit allows to extract β and η, respectively the shape parameter and the scale parameter of the cumulative failure fraction f assumed to

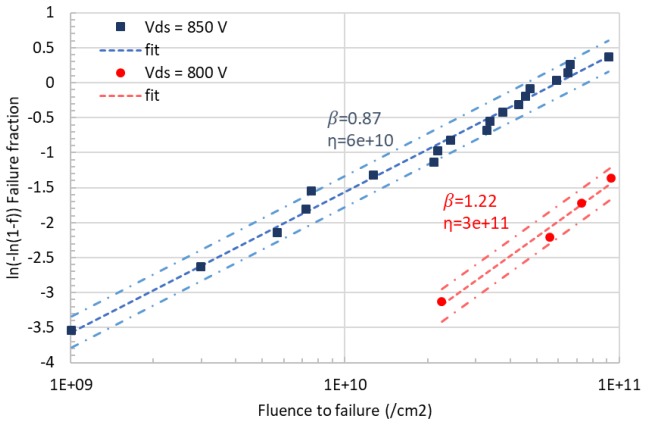

Fig. 9. Weibull plots at Vds = 850 V and Vds = 800 V for proton data.

be of the Weibull type given by:

$$f(\Phi) = 1 - e^{-(\frac{\Phi}{\eta})^{\beta}} \quad (1)$$

The value of β is close to unity for both curves, which is the expected value for a random failure mechanism (i.e. no cumulative degradation). The fact that only 4 devices were destructed at 800V confirms that this voltage is only slightly above the safe-operating area (SOA) threshold.

B. Atmospheric neutron destructive test results

Fig. 10 presents the sum of the drain and gate currents of the 32 devices exposed in parallel during the first neutron campaign at Vds=850V, with each correlated steps indicating a failure (Ids steps non-correlated with Igs steps came from another test board and are therefore not to be taken into account in this work). Indeed, all the destructed devices presented both a drain-source and a gate-source short-circuit as a result of the catastrophic failure. Due to the limited time resolution of the current measurements in such electrical setup, it is not possible to determine which of the two current increases first. It seems reasonable to consider that the melting of a source contact locally induced by an SEB-like failure could produce a short with the nearest gate. Whether an SEGR-like failure could produce the observed electrical signature still needs to be clarified by failure analysis of the destructed samples.

Because of the distance between the beam output and the DUTs, and because several test boards were stacked in the beam in front of the devices of interest (Fig. 7), the neutron spectrum

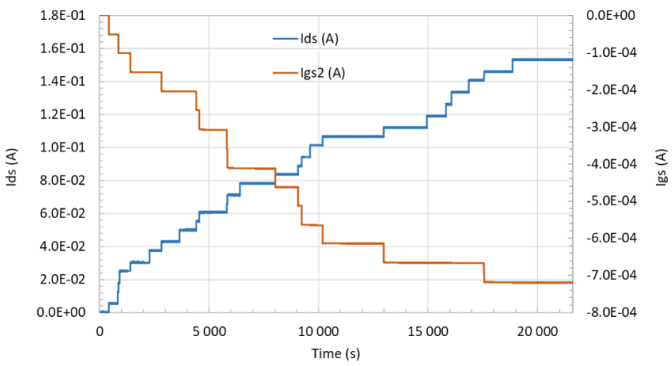

Fig. 10. Typical currents acquisition results under neutron at Vds=850V.

transformation or attenuation through the stack of materials has to be considered accurately to estimate the effective fluence at each DUT location [8-9]. Several simple attenuation models were considered :

- Model 0: only the beam output divergence is considered.
- Model 1: the attenuation through the stack of screening materials is calculated for an average neutron energy of 200MeV and considered to be constant over the whole spectrum.
- Model 2: the attenuation is calculated in multiple energy ranges from thermal energy up to 100MeV using [10]. The attenuation of neutrons with energies higher than 100MeV is assumed to be negligible.
- Model 3: same as Model 2 except that the attenuation is calculated in range 10-800MeV (thermal energies excluded) using [10] between 10 and 200MeV and a constant attenuation from 200 to 800MeV.

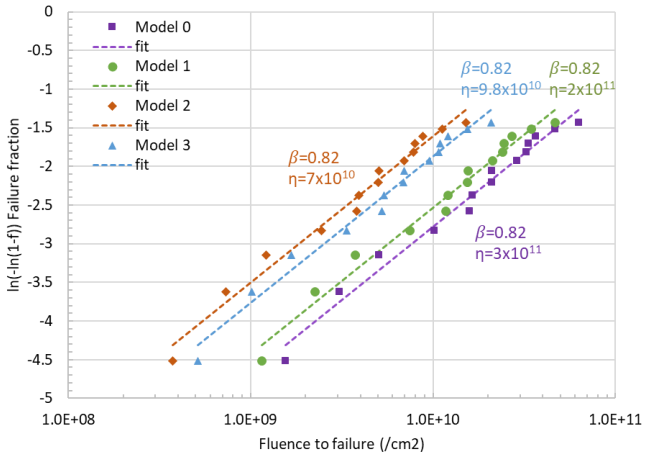

Fig. 11. Weibull plots at Vds = 850 V for neutron data, with different models of the beam attenuation.

Models 2 and 3 are expected to be the most realistic ones but only a detailed Monte-Carlo analysis of the experimental setup could be conclusive on this point. Weibull plots of the results are presented in Fig. 11. As for protons, the shape parameter is consistent with random destructive events. For the scale parameter, a factor of 3 is found between the uncorrected (model 0) and corrected (model 3) fluences to failure, confirming the importance of modelling the beam attenuation in a stacked board setup.

C. Atmospheric neutron non-destructive test results

The results of the non-destructive transient acquisitions for different Vds voltages during the first neutron campaign are presented in Fig 12. One can clearly observe a change of slope for SETs with an amplitude larger than 0.25V for the different drain voltages. This change in the slope allows to extract an estimation of the SEB cross section in the saturated region, which is estimated to be around 5 10^{-10}cm² from Fig. 12.

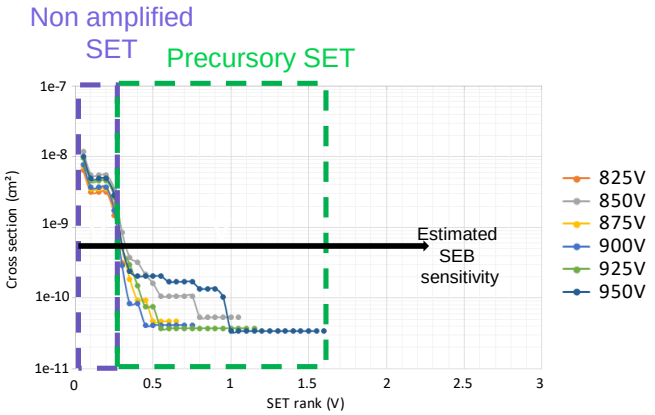

Fig. 12. Distribution of single-event transients amplitude obtained by the non-destructive test method for different drain voltages.

IV. Results Correlation & Discussion

Fig. 13 presents the destructive proton and neutron test results on the same Weibull plot. For the neutron, the model 2 of the beam attenuation is used in this plot, but the model 3 would only slightly offset the neutron data points towards the right.

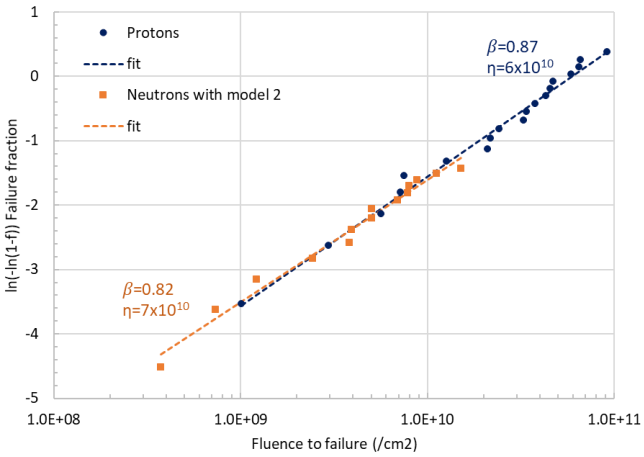

Fig. 13. Weibull plots at Vds = 850 V for neutron and proton data considering model 2 for neutrons fluence correction.

The correlation of the proton and neutron results is excellent, confirming that testing with high-energy protons is a reliable alternative to a standard atmospheric-neutron test for this technology. From the Weibull plots, the cross section is given by the inverse of the mean fluence to failure, that is:

$$\sigma = \left[\eta\, \Gamma\left(1+\frac{1}{\beta}\right)\right]^{-1} \qquad (2)$$

Table I presents the destructive single-event cross section extracted from the different test methods. Note that for the neutron non-destructive and destructive test at 1050V (second campaign), all devices were exposed in front of the beam output so no beam attenuation had to be considered.

First looking at the destructive test results at 850V, it appears that the destructive proton test provides a slightly conservative value of the neutron cross section that is totally within the statistical error bars for such measurements. The destructive neutron test performed at 1050V provide a higher value because this voltage is much beyond the SOA limit of this device

Table I: Cross sections per method

Test method	Extracted Cross Section (cm²)
Destructive at 850V, 194MeV protons	$1.6\ 10^{-11}$
Destructive at 850V, neutrons (attenuation model 2)	$1.3\ 10^{-11}$
Destructive at 850V, neutrons (attenuation model 3)	$9.2.10^{-12}$
Destructive at 1050V, neutrons (no attenuation)	$5.6.10^{-10}$
Non-destructive, 194MeV protons	3.10^{-10}
Non-destructive, neutrons (no attenuation)	5.10^{-10}

(estimated to be close to 800V from the investigation runs described in section II-F), so the measured cross section at 1050V is probably closer to the saturated part of the cross section vs drain voltage curve for the 1200V device tested in this work.

The cross section evaluations extracted from the non-destructive test results are conservative when compared to the 850V destructive test results, and in good agreement with the 1050V destructive test results. This result demonstrates the efficiency of the non-destructive test method for a preliminary assessment of the SOA and the destructive events cross section of a SiC power device. The small difference between the proton and neutron cross sections extracted from the non-destructive tests is not significant in the context of such preliminary assessment.

V. TCAD modelling

In order to investigate the failure mechanisms at play in the tested device, 2D TCAD simulations of the elementary MOSFET structure presented in Fig. 14 were performed using the ECORCE software [12]. The geometrical and physical parameters of the structure were adjusted, starting from a construction analysis of a sample, in order to fit the main static electrical characteristics measured on a real device.

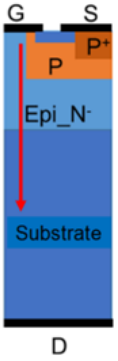

Fig. 14. Simplified schematic of the simulated SiC MOSFET structure.

The structure irradiation was then simulated by injecting various ion charge generation tracks associated to secondary products from neutron interaction, using different positions in the structure as the starting point of the track as well as different directions and linear energy transfer (LET) corresponding to the ion types and energies resulting from these interactions.

Fig 15 presents an example of the results regarding the redistribution of the potential and electric field in the structure during an event producing an ion track that crosses the epitaxial

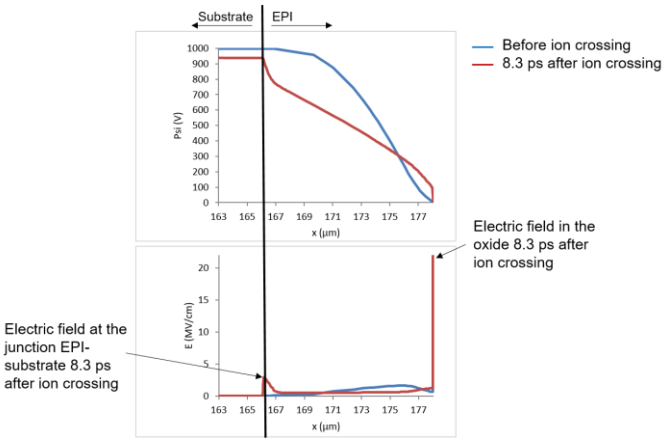

Fig. 15. Potential (top) and electric field (bottom) distribution along a vertical line below the gate, before and during an ion impact depicted by the red arrow of Fig. 14. The maximum x coordinate corresponds to the SiC/gate oxide interface. (EPI: epitaxial layer)

layer towards the substrate, as illustrated by the red arrow on Fig. 14. Due to the conductive path formed by the ion track, a significant part of the potential difference between the drain and the source is transferred towards the top of the epitaxial layer, in the vicinity of the gate oxide. This results in a significant increase of the electric field in the gate oxide as can be seen in Fig 15-bottom. In this example, such electric field could induce a breakdown of the oxide, leading to an SEGR-like failure.

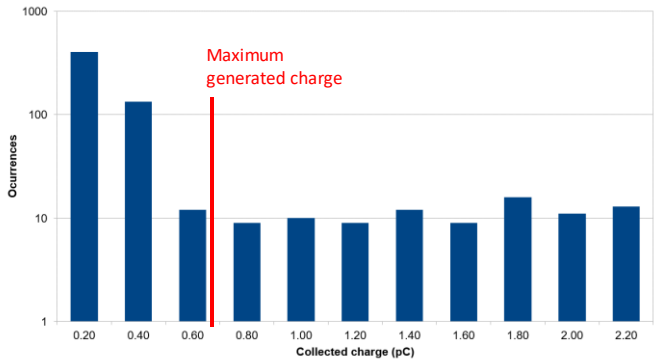

Fig. 16. Histogram of collected charge for 640 simulations of the structure at Vds=1000V with a 32MeV Na ion track of various starting points and directions. The red line shows the maximum charge that can be generated by this ion in the structure.

Note in Fig 15 that the electric field also increases at the substrate-side of the epitaxial layer to a level that is slightly higher than the critical field required to trigger impact ionization in SiC (3MV/cm), leading to an amplification of the collected charge. Fig. 16 presents the histogram of the drain collected charge for 640 simulations of the structure with a 32MeV Na ion track injected with regularly distributed positions and directions. The maximum charge that can be generated by this ion when its track is completely contained within the simulated structure is 0.67pC. One can observe that a number of tracks (approximately 14%) lead to a collected charge higher than this maximum generation. Depending on the track starting point and direction, these charge amplification events were associated either to the contribution of impact ionization or to the track temporarily acting as a conductive shunt between the source and the epitaxial region. Such events could be the precursory of an SEB-like failure, although no catastrophic runaway was observed in any of our simulations with this structure, as it was in previous works for a different SiC device with the same simulation models [13]. The fact that the non-destructive technique based on transients amplification provides a good estimation of the destructive events cross section and the failure electrical signatures that were observed experimentally are both compatible with an SEB-like failure. The fact that our simulations did not show such behavior could well be explained by the lack of available details on the doping profiles of the real structure. Still, the simulations did confirm the possibility of charge amplification within the structure.

VI. CONCLUSIONS

High-energy proton and atmospheric neutron tests results obtained for a recent 1200V SiC MOSFET with the classical statistical destructive method and a non-destructive approach were presented and compared. Results show the importance of accurately modelling the neutron fluence attenuation in a stacked-boards setup, and confirm that high-energy proton testing is a reliable method for evaluating this technology for atmospheric applications. The non-destructive method is found to provide a conservative estimation of the saturated cross section, confirming the interest of the approach when only few devices are available (statistical approach is then not an option) or if the beam time is constrained. TCAD simulations of a structure fitting the electrical performances of the tested device were performed, showing the possibility of both oxide damage and charge amplification in the structure.

VII. REFERENCES

[1] A. F. Witulski et al., "Single-Event Burnout Mechanisms in SiC Power MOSFETs," in IEEE Transactions on Nuclear Science, vol. 65, no. 8, pp. 1951-1955, Aug. 2018, doi: 10.1109/TNS.2018.2849405.

[2] P. Fabio et al, "Investigation of the Impact of Neutron Irradiation on SiC Power MOSFETs Lifetime by Reliability Tests", Sensors 21, no. 16: 5627, 2021

[3] C. Martinella et al., "Impact of Terrestrial Neutrons on the Reliability of SiC VD-MOSFET Technologies", IEEE Trans. Nucl. Sci., vol. 68, no. 5, pp. 634-641, May 2021, doi: 10.1109/TNS.2021.3065122.

[4] K. Niskanen et al., "Impact of Electrical Stress and Neutron Irradiation on Reliability of Silicon Carbide Power MOSFET," in IEEE Trans. Nucl. Sci., vol. 67, no. 7, pp. 1365-1373, July 2020.

[5] A. Akturk et al., "Energy Dependence of Atmospheric Neutron-Induced Failures in Silicon Carbide Power Devices," in IEEE Trans. Nucl. Sci., vol. 69, no. 4, pp. 900-907, April 2022, doi: 10.1109/TNS.2022.3154394.

[6] V. Ferlet-Cavrois et al., "Statistical Analysis of Heavy-Ion Induced Gate Rupture in Power MOSFETs—Methodology for Radiation Hardness Assurance," IEEE Trans. Nucl. Sci., vol. 59, no. 6, pp. 2920-2929, Dec. 2012, doi: 10.1109/TNS.2012.2223761.

[7] A. Touboul et al., Neutrons-Induced IGBT Failure: Effects of the Number of Tested Devices on the Cross Section Calculation, IEEE Trans. Nucl. Sci., vol. 60-4, August 2013

[8] F. Miller, S. Morand, A. Douin, R. Gaillard, T. Carriere and N. Buard, "Laser Validation of a Non-Destructive Test Methodology for the Radiation Sensitivity Assessment of Power Devices," in IEEE Trans. Nucl. Sci., vol. 58, no. 3, pp. 813-819, June 2011, doi: 10.1109/TNS.2010.2098887.

[9] S. A. Wender, J. M. O'Donnell, L. Zavorka and B. L. Bhuva, "Neutron Beam Attenuation Through Semiconductor Devices During SEU Testing," 2019 IEEE IRPS, 2019, pp. 1-4, doi: 10.1109/IRPS.2019.8720477.

[10] D. Chiesa et al., "Measurements of Neutron Fields in a Wide Energy Range Using Multi-Foil Activation Analysis," IEEE Trans. Nucl. Sci., vol. 69, no. 7, pp. 1659-1666, July 2022, doi: 10.1109/TNS.2021.3138636..

[11] F. Wrobel, "Detailed history of recoiling ions induced by nucleons," Computer Physics Communications, vol. 178, no. 2, pp. 88–104, Jan. 2008
[12] A. Michez, S. Dhombres, J. Boch, "ECORCE: A TCAD Tool for Total Ionizing Dose and Single Event Effect Modeling," IEEE Trans. Nucl. Sci., vol. 62, no. 4, pp. 1516-1527, Aug. 2015, doi: 10.1109/TNS.2015.2449281.
[13] S. Kuboyama et al., "Thermal Runaway in SiC Schottky Barrier Diodes Caused by Heavy Ions," in IEEE Transactions on Nuclear Science, vol. 66, no. 7, pp. 1688-1693, July 2019, doi: 10.1109/TNS.2019.2914494.